

Coulomb explosion of N_2 and CO_2 using linearly and circularly polarized femtosecond laser pulses

Ph. Hering and C. Cornaggia

CEA Saclay/Direction des Sciences de la Matière, Service des Photons, Atomes et Molécules, Bâtiment 522,
F-91 191 Gif-Sur-Yvette, France

(Received 23 October 1998)

Laser-induced molecular coulomb explosion of N_2 and CO_2 is studied experimentally using linearly and circularly polarized laser light in the 10^{15} W/cm^2 intensity range at $\lambda = 800 \text{ nm}$. The fragmentation kinetic energy releases are found to be identical in both cases using two different experimental methods. These results show that the molecular relaxation is independent of the respective directions of the laser electric field and of the internuclear axis. These results are confirmed by varying the linear laser polarization direction relative to the explosion direction of N_2 and CO_2 . Moreover, since in the linear case the molecular reorientation occurs along the laser electric field direction, these results show that inertial effects are not responsible for the possible elongation of the internuclear distances. [S1050-2947(99)06103-X]

PACS number(s): 33.80.Rv, 33.80.Eh, 42.50.Vk

I. INTRODUCTION

Laser-induced multiple ionization of molecules produces multicharged atomic ions due to the relaxation of the transient multicharged molecular ions [1]. At the beginning of the 1990s, experiments performed with light molecules such as N_2 , O_2 , CO , and C-C bonds indicate that the kinetic energy releases exhibit only one maximum per fragmentation channel which is a fraction of Coulomb explosion energy [2–4]. In addition, this fraction does not depend drastically on the decay channel, wavelength, and pulse duration. These studies were extended to molecules built with heavier atoms such as Cl_2 [5] or I_2 [6] and gave essentially the same conclusions. One of the possible explanations is that the molecular explosion occurs at a larger internuclear distance than the equilibrium distance. Recent theoretical models based on the over-the-barrier ionization [7] and on a full quantum treatment [8] explain this behavior by an enhancement of the molecular ionization at a critical larger internuclear distance which is poorly dependent on the ionization stage. Although these two approaches are quite different, their common interpretation is based on the nonadiabatic localization of the electronic wave function in the rising well of the laser-molecule potential. In addition, the concept of charge resonance effects in strong laser fields was introduced in the early 1990s [9] and has been applied to the multiple ionization of small molecules [10]. In this approach, the enhancement at large internuclear distance is due to charge resonance states that are responsible for very large transition moments. On the other hand, Brewczyk *et al.* have developed a time-dependent Thomas-Fermi model and found that the kinetic energy defect is due to screening processes of the departing electrons [11,12]. According to the authors, this new model does not attribute much importance to the enhanced ionization at some critical distance.

In all these approaches the laser light is linearly polarized because there do not exist any data recorded with circularly polarized laser light. Moreover, the calculations are performed assuming that the internuclear axis lies along the

laser electric field direction. In this paper, the relaxation of N_2 and CO_2 is investigated in the 10^{15} W/cm^2 laser intensity range at $\lambda = 800 \text{ nm}$ in linear and circular polarization in order to give more experimental information especially where two- and three-dimensional models are required to treat the circularly polarized laser light. In the models involving an enhancement at large internuclear distances [7–10], the stretching processes leading to these large distances have not been identified. In the case of linear polarization, the light molecules such as H_2 , N_2 , or CO get aligned along the laser electric field [13–15] and an inertial effect might increase the internuclear distance. In the case of circular polarization, the molecular axis cannot follow the rotation of the laser field during the laser period $T = 2.67 \text{ fs}$ at $\lambda = 800 \text{ nm}$. As a consequence, inertial effects are not expected to play any significant role. In addition, the molecular axis is no longer aligned along the laser electric field. Concerning the Thomas-Fermi approach [11,12], the dynamics of the departing electrons has been investigated only using linear polarization. Since it is expected to be different in circular polarization at first sight, the model will have to be checked in this case.

This paper is based on the detection of the fragmentation channels of N_2 and CO_2 into multicharged atomic fragments and on the comparison of the experimental results recorded with linear and circular polarization. The paper is organized as follows. Section II describes the experimental setup. In particular, Sec. II C presents a detailed description of the two experimental methods used for the measurements of the kinetic energy releases. The experimental results are presented in Sec. III and are discussed in Sec. IV.

II. EXPERIMENTAL SETUP

A. Laser setup

The femtosecond laser system is a commercial kilo-Hertz laser chain based on a titanium-sapphire gain medium. A self-mode-locked oscillator pumped by an Ar^+ cw laser delivers pulses with a wavelength spectrum centered at λ

=800 nm and pulse duration $\tau=27$ fs. The amplification is performed using the chirp pulse amplification technique: the laser pulse from the oscillator is stretched to a pulse duration $\tau=300$ ps, then the amplification takes place in a regenerative amplifier pumped by a kHz-Nd³⁺:YLF laser. Finally, the pulse duration is recompressed to typically $\tau=40$ fs using a two-grating compressor. The laser pulse duration is measured using standard optical second-order autocorrelation techniques. The laser system output at 1 kHz is typically 750 μ J at $\lambda=800$ nm.

B. Ion time-of-flight spectrometer and correlation technique

The laser-induced molecular multifragmentation takes place in a high vacuum chamber with a residual pressure of 3×10^{-10} Torr. The multicharged atomic and molecular ions are detected using a Wiley-McLaren ion spectrometer [16], with a short time-of-flight drift tube (100 mm) in order to avoid any angular discrimination using a moderate collection electric field. The spectrometer is operated so that the time-of-flight difference $T(\mathbf{P}) - T(\mathbf{P}=\mathbf{0})$ of an ion with initial momentum \mathbf{P} exhibits to a very good approximation a linear dependence of the projection $P \cos(\vartheta)$ of \mathbf{P} along the spectrometer axis:

$$T(\mathbf{P}) - T(\mathbf{P}=\mathbf{0}) = P \cos(\vartheta) / (ZeF_c), \quad (1)$$

where Z is the ion charge state, e is the elementary charge, and F_c is the collection electric field. The ions are detected by a pair of microchannel plates and the resulting ion signal is transferred to a digitizing oscilloscope. The gas pressure remains very low in the 10^{-9} – 10^{-8} Torr range in order to keep a linear response of the detector as a function of the number of the impinging ions.

The fragmentation channels are established using the covariance mapping technique introduced by Frasinski *et al.* [17], which allows us to work with more than one event per laser shot. In the case of diatomic molecules, only the second-order covariance coefficient $C_2(T_1, T_2)$ is required to associate two atomic ions with times of flight T_1 and T_2 . For triatomic molecules, the third-order covariance coefficient $C_3(T_1, T_2, T_3)$ is necessary to identify channels with three ions. However, this coefficient is always much smaller than $C_2(T_1, T_2)$ and demands more computation time. As a consequence, both coefficients are used and discussed in this paper for CO₂.

C. Experimental method

The molecular alignment along the laser electric field was established previously using linear polarization [13–15]. In the case of the circular polarization, the multifragmentation is isotropic in space [18]. In this case, two methods are used to measure to kinetic energy releases. In the first one, 90% high transparency grids are installed in the spectrometer to collect all the ions. Figure 1 represents the covariance map recorded with the N₂ molecule for the identification of the N^{Z+} + N^{Z'+} ($Z, Z' = 2, 3$) channels. The bottom and left curves represent, respectively, the T_1 and T_2 time-of-flight average ion signal and the central map represents the $C_2(T_1, T_2)$ coefficient using a five-level gray scale. The ion collection electric field is $F_c = 180$ V/cm and the laser linear

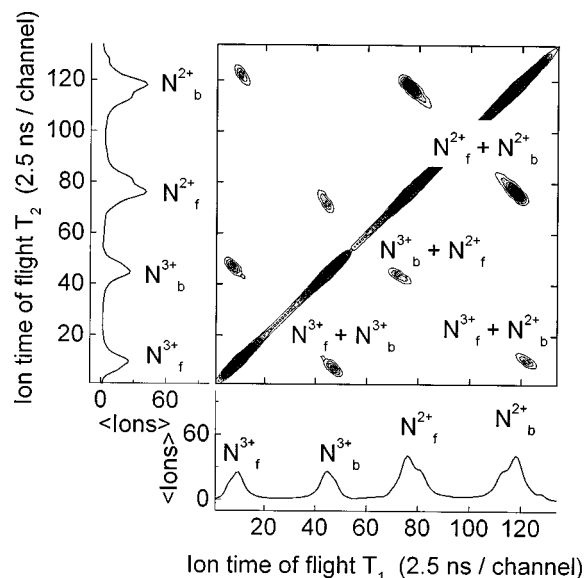


FIG. 1. Covariance map of N₂ recorded at $\lambda=800$ nm, $I=4 \times 10^{15}$ W/cm², and $p(\text{N}_2)=1.5 \times 10^{-9}$ Torr with the laser polarization direction parallel to the detection axis. The spectrometer is equipped with high transparency grids. The collection electric field is $F_c=180$ V/cm. The covariance coefficient $C_2(T_1, T_2)$ is represented using a five-level gray scale as a function of the T_1 (horizontal axis) and T_2 (vertical axis) ion times of flight.

polarization direction is parallel to the spectrometer axis. Since the molecule is aligned along the laser electric field, the N^{Z+} ions are ejected along the spectrometer axis and present a highly symmetric double peak structure coming from the backward (N_b^{Z+}) and the forward (N_f^{Z+}) initial emission directions relative to the detector position. Figure 2

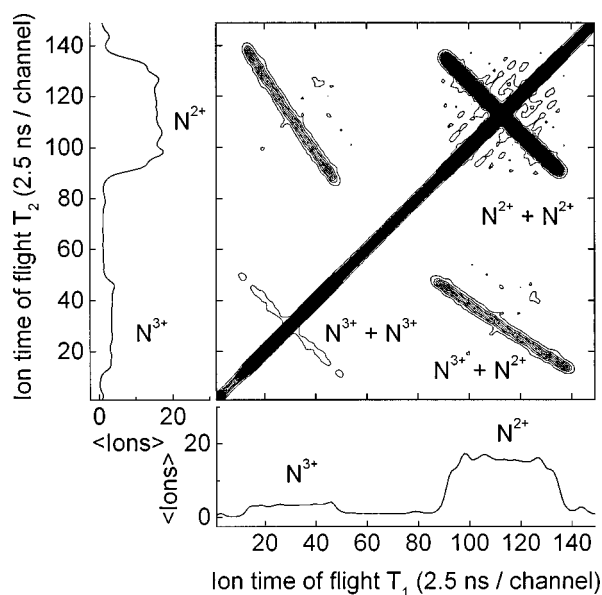


FIG. 2. Covariance map of N₂ recorded at $\lambda=800$ nm, $I=4 \times 10^{15}$ W/cm², and $p(\text{N}_2)=2 \times 10^{-9}$ Torr with circular laser polarization. The spectrometer is equipped with high transparency grids. The collection electric field is $F_c=180$ V/cm. The covariance coefficient $C_2(T_1, T_2)$ is represented using a five-level gray scale as a function of the T_1 (horizontal axis) and T_2 (vertical axis) ion times of flight.

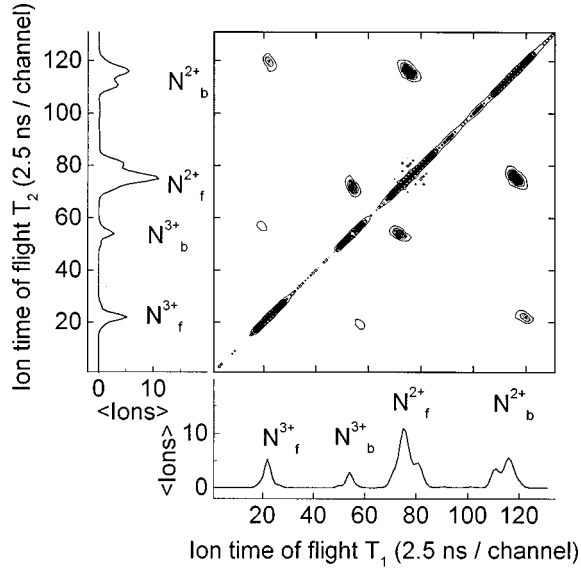


FIG. 3. Covariance map of N_2 recorded at $\lambda=800$ nm, $I=3 \times 10^{15}$ W/cm 2 , and $p(N_2)=4 \times 10^{-9}$ Torr with the laser polarization direction parallel to detection axis. The spectrometer is equipped with a 1 mm pinhole for an on-axis detection. The collection electric field is $F_c=100$ V/cm. The covariance coefficient $C_2(T_1, T_2)$ is represented using a five-level gray scale as a function of the T_1 (horizontal axis) and T_2 (vertical axis) ion times of flight.

represents a map recorded with the same operating conditions of the ion spectrometer and is recorded using circular laser polarization. The N^{2+} and N^{3+} ion peaks in the time-of-flight spectra exhibit a square shape due to their initial isotropic emission. Indeed, the ion distribution $D_{\mathbf{P}}(\mathbf{P})$ depends only on the modulus P of the vector momentum \mathbf{P} . Assuming that this distribution is a narrow distribution $D_{\mathbf{P}}(\mathbf{P})=\delta(P-P_0)$ centered at P_0 , the ion distribution $D_T(T)$ as a function of the time of flight $T(\mathbf{P})$ is a square centered at $T(\mathbf{P}=\mathbf{0})$ with a symmetric maximum extension at $\pm P_0/ZeF_c$. This statement comes from the $D_{\mathbf{P}}(\mathbf{P})d\mathbf{P}=D_T(T)dT$ equality and the $P \cos(\vartheta)$ dependence of $T(\mathbf{P})$ given in Eq. (1). The $N^{Z+}/N^{Z'+}$ ($Z, Z'=2,3$) covariance islands are straight lines with constant $C_2(T_1, T_2)$ values. The slopes are Z'/Z because of the $\mathbf{P}+\mathbf{P}'=\mathbf{0}$ momentum conservation which is equivalent to $ZT(N^{Z+})+Z'T(N^{Z'+})=\text{const}$ following Eq. (1).

The second method is based on the analysis of the fragmentation along the spectrometer axis. The high transmission grid of the ion collection region is replaced by a flat disk with a small hole at the center. In this paper, we present results obtained with a 1 mm diameter hole. Figures 3 and 4 represent covariance maps recorded with an $F_c=100$ V/cm collection electric field using, respectively, linear and circular polarization for the same channel identification as in Figs. 1 and 2. For the linear polarization (Fig. 3), the forward and backward ions pass through the hole since the molecular axis is aligned along the spectrometer axis by the laser field. However, the backward ion peaks are smaller than the forward ion peaks because of the different trajectories of these two ion species in the collection electric field. In the case of circular polarization (Fig. 4), the molecular fragmentation is detected for molecules with internuclear axis along the spectrometer axis, otherwise the ions do not pass through the

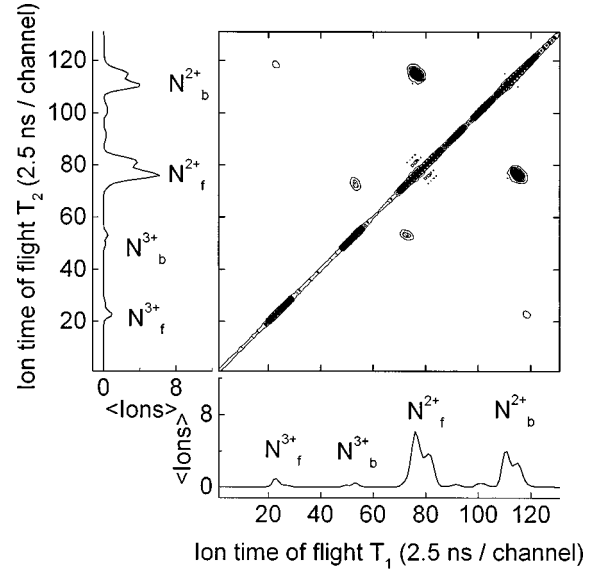


FIG. 4. Covariance map of N_2 recorded at $\lambda=800$ nm, $I=3 \times 10^{15}$ W/cm 2 , and $p(N_2)=4 \times 10^{-9}$ Torr with circular laser polarization. The spectrometer is equipped with a 1 mm pinhole for an on-axis detection. The collection electric field is $F_c=100$ V/cm. The covariance coefficient $C_2(T_1, T_2)$ is represented using a five-level gray scale as a function of the T_1 (horizontal axis) and T_2 (vertical axis) ion times of flight.

hole. The covariance map looks like the map in Fig. 3 with some differences in the intensities of the covariance peaks, which will be explained in the next section.

Both methods give the same important results: the fragmentation channel kinetic energy releases are identical in linear and circular polarization. The ion kinetic energies are slightly higher using the on-axis detection (pinhole) than using the total detection (grids). The differences lie in the 0–1.5 eV range depending on the fragmentation channel and remain in the $\Delta E/E=\pm 5\%$ relative uncertainty.

III. EXPERIMENTAL RESULTS

A. N_2

Table I summarizes the kinetic energy releases for the $N^{Z+}+N^{Z'+}$ fragmentation channels of N_2 using linearly and

TABLE I. Measured kinetic energy releases E_{exp} of the $N^{Z+}+N^{Z'+}+E_{\text{exp}}$ channels from the N_2 molecule using linearly and circularly polarized laser light at $\lambda=800$ nm, 40 fs pulse duration in the 10^{15} – 5×10^{15} W/cm 2 laser intensity range. The relative accuracy of the measurements is $\Delta E/E=\pm 5\%$. These results come from covariance maps recorded using the on-axis detection. The Coulomb repulsion energy E_{Coul} is calculated at the N_2 equilibrium internuclear distance $R_e=1.098$ Å.

(Z, Z')	Experimental kinetic energy release E_{exp} (eV)	$E_{\text{exp}}/E_{\text{Coul}}$ (%)
(1,1)	7.6 ± 0.5	58
(2,1)	15 ± 1	57
(2,2)	29 ± 1.5	55
(3,2)	40 ± 2	51
(3,3)	56 ± 3	47

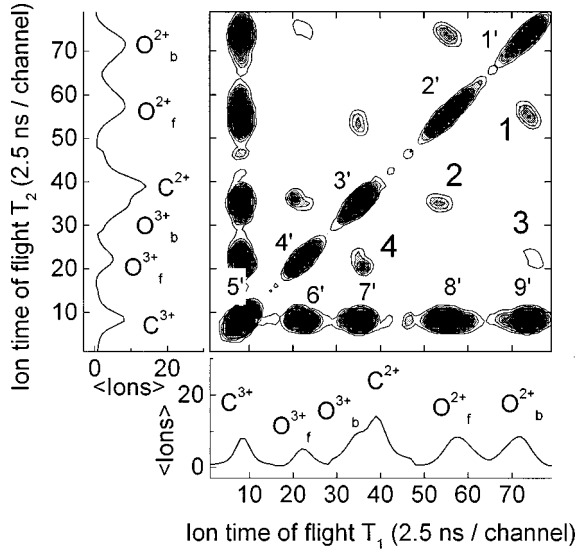


FIG. 5. Third-order covariance map of CO₂ recorded at $\lambda = 800$ nm, $I = 4 \times 10^{15}$ W/cm², $p(\text{CO}_2) = 10^{-9}$ Torr, and linear polarization with the ion spectrometer equipped with grids. The collection electric field is $F_c = 500$ V/cm. The $C_3(T_1, T_2, T_3)$ coefficient is represented with a fixed $T_3 = T_3^{(0)}$ value which corresponds to zero-kinetic-energy C³⁺ ions. The islands labeled 1'–9' correspond to a partial autocorrelated signal with $T_1 = T_2$ (1'–5') and $T_2 = T_3^{(0)}$ (5'–9') and are commented on in the text. The channels identification is as follows: Island 1; O_f²⁺ + C³⁺ + O_b²⁺; island 2, O_b³⁺ + C³⁺ + O_f²⁺; island 3, O_f³⁺ + C³⁺ + O_b²⁺; island 4, O_f³⁺ + C³⁺ + O_b³⁺.

circularly polarized laser light and the on-axis detection. The experimental values E_{exp} reported in Table I are average values over several covariance maps as in Figs. 3 and 4 using different collection electric fields F_c from 50 to 200 V/cm. These quantities are represented with only two significant digits which are sufficient within the experimental relative accuracy $\Delta E/E = \pm 5\%$. The experimental kinetic energy releases E_{exp} are compared to the Coulomb repulsion energy E_{Coul} . For the different fragmentation channels, the ratio $E_{\text{exp}}/E_{\text{Coul}}$ values are around 50%, as was outlined using a linearly polarized 2 ps laser pulse at 616 nm [4]. The kinetic energy releases recorded with circularly polarized laser light do not differ significantly from the results recorded with linear polarization and do not require another column in Table I since the E_{exp} values are the same in both cases within the experimental accuracy. The two-dimensional spectra were recorded using the same laser intensity with grids in Figs. 1 and 2 ($I = 4 \times 10^{15}$ W/cm²) and with the 1 mm pinhole in Figs. 3 and 4 ($I = 3 \times 10^{15}$ W/cm²). However, in each case the peak intensities of the N³⁺ ions and of the associated N³⁺/N³⁺ correlation island are smaller using the circular polarization. In this last case, the multiple ionization is less efficient because the laser electric field is $\sqrt{2}$ smaller in circular polarization than in linear polarization for the same laser intensity.

B. CO₂

Figure 5 represents a third-order covariance map recorded with the C²⁺, C³⁺, O²⁺, and O³⁺ ions using linear polarized laser light and high transparency grids in the ion spectrom-

TABLE II. Measured kinetic energy releases E_{exp} of the O^{Z+} + C^{Z'+} + O^{Z''+} + E_{exp} channels from the CO₂ molecule using linearly and circularly polarized laser light at $\lambda = 800$ nm, 40 fs pulse duration in the $10^{15} - 5 \times 10^{15}$ W/cm² laser intensity range. The relative accuracy of the measurements is $\Delta E/E = \pm 10\%$. These results are average values coming from second-order $C_2(T_1, T_2)$ covariance maps recorded with pinholes and third-order $C_3(T_1, T_2, T_3)$ covariance maps recorded with grids as it is explained in the experimental section. The Coulomb repulsion energy E_{Coul} is calculated at the C-O equilibrium internuclear distance of the CO₂ molecule $R_e(\text{C-O}) = 1.162$ Å.

(Z, Z', Z'')	Experimental kinetic energy release E_{exp} (eV)	$E_{\text{exp}}/E_{\text{Coul}}$ (%)
(1,1,1)	18±2	55
(1,2,1)	34±3.5	61
(2,1,1)	27±3	54
(2,1,2)	38±4	51
(2,2,2)	68±7	55
(2,3,2)	90±9	52
(3,2,2)	89±9	55
(3,3,2)	109±10	49
(3,3,3)	143±14	51

eter. As usual, the bottom and left curves represent the average ion time-of-flight signal. In particular, the backward component O_b³⁺ of the O³⁺ ion lies in the left shoulder of the C²⁺ ion peak which exhibits a single peak structure (as the C³⁺ ion peak) because the carbon atom occupies the central position of the CO₂ molecule. The third-order coefficient $C_3(T_1, T_2, T_3)$ is represented using a two-dimensional map with a fixed $T_3 = T_3^{(0)}$ time of flight which corresponds to C³⁺ ions with zero initial momentum $P=0$ along the spectrometer axis. This situation gives the highest values of the C_3 coefficient especially for symmetric channels such as O²⁺ + C³⁺ + O²⁺ and O³⁺ + C³⁺ + O³⁺. This is the signature that the three-body multifragmentation of CO₂ is a direct process, otherwise the C³⁺ would have some initial kinetic energy due to the departure of a daughter CO^{N+} fragment. The same behavior is observed with the C²⁺ ion, where $T_3^{(0)}$ corresponds to the time of flight of C²⁺ ions with initial momentum $P=0$. As for the $C_2(T_1, T_2)$ coefficient, the $C_3(T_1, T_2, T_3 = T_3^{(0)})$ coefficient is symmetric with respect to T_1 and T_2 and only the features below the diagonal are commented upon. The diagonal islands 1'–5' represent the partial autocorrelated $C_3(T_1, T_2 = T_1, T_3 = T_3^{(0)})$ coefficient. The C³⁺ ion peak is correlated with the O_f³⁺, O_b³⁺, O_f²⁺, and O_b²⁺ ions. In particular, island no. 3' is centered around the O_b³⁺ ion because the C³⁺ ion cannot be correlated with the C²⁺ ion. The horizontal islands 6'–9' represent the partial autocorrelated $C_3(T_1, T_2 = T_3^{(0)}, T_3 = T_3^{(0)})$ coefficient which gives the same identification as with the diagonal islands. Finally islands no. 1–4 with three distinct times of flight give the identification and kinetic energy releases for the O^{Z+} + C³⁺ + O^{Z'+} ($Z, Z' = 2, 3$) channels which are reported in Table II.

Figures 6 and 7 represent second-order covariance maps recorded with a 1 mm pinhole in the ion spectrometer using,

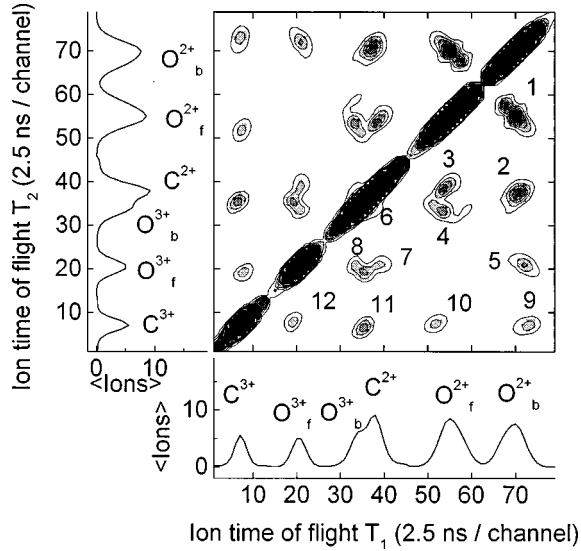


FIG. 6. Second-order covariance map of CO_2 recorded at $\lambda = 800$ nm, $I = 4 \times 10^{15}$ W/cm 2 , $p(\text{CO}_2) = 4 \times 10^{-9}$ Torr, and linear polarization with the ion spectrometer equipped with a 1 mm pinhole for an on-axis detection. The collection electric field is $F_c = 500$ V/cm. Islands 1, 4, 5, and 8 correspond to $\text{O}^{Z+}/\text{O}^{Z'++}$ correlations and islands 2, 3, and 9–12 correspond to $\text{O}^{Z+}/\text{O}^{Z'++}$ correlations with $Z, Z' = 2, 3$.

respectively, linearly and circularly polarized laser light. In this case, the multifragmentation is detected for molecules oriented along the ion detection axis. The same island patterns are detected in both cases and are labeled in the figure captions from 1 to 12. Third-order covariance mapping is more difficult with the pinhole ion discrimination and the C_3 signal is very weak compared with the C_3 signal obtained with grids. The equivalence of the kinetic energy releases in both polarization states is illustrated here with doubly and triply charged atomic ions but has been checked also with

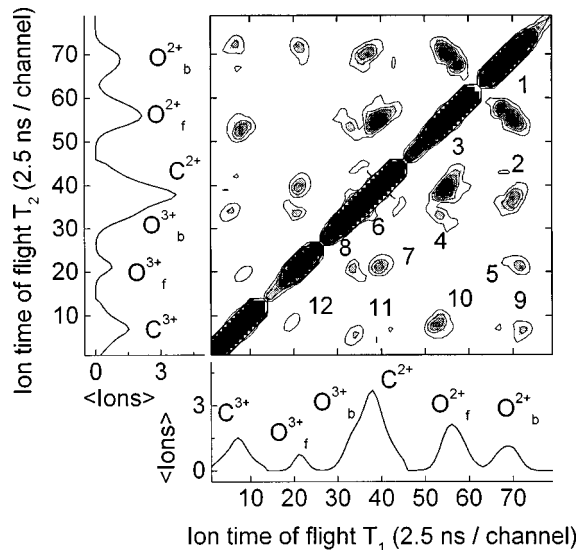


FIG. 7. Second-order covariance map of CO_2 recorded at $\lambda = 800$ nm, $I = 4 \times 10^{15}$ W/cm 2 , $p(\text{CO}_2) = 4 \times 10^{-9}$ Torr, and circular polarization with the ion spectrometer equipped with a 1 mm pinhole for an on-axis detection. The collection electric field is $F_c = 500$ V/cm. The island labels are the same as in Fig. 6.

singly charged atomic ions. The energies are summarized in Table II and represent average values of several two-order and three-order covariance maps using the on-axis detection and the grid configuration of the ion spectrometer. The relative accuracy $\Delta E/E = \pm 10\%$ is larger for CO_2 than for N_2 because the CO_2 experiments (Figs. 5–7) are performed using a larger collection electric field $F_c = 500$ V/cm in order to collect all the ions especially for the triple-correlation experiments [$\Delta E/E$ is proportional to F_c according to Eq. (1)]. As in the case of N_2 , the kinetic energy releases are identical in both polarization states and the correlation islands in Fig. 7 are less intense (circular polarization) than in Fig. 6 (linear polarization) because of the $\sqrt{2}$ smaller laser electric field in circular polarization for the same laser intensity.

IV. DISCUSSION

In the linearly polarized laser light case, the N_2 and CO_2 molecules are aligned along the laser electric field direction and undergo multiple ionization and Coulomb explosion. This statement is in good agreement with the recent experimental and theoretical study of Posthumus *et al.* where molecules built with light atoms such as H_2 or N_2 show clear signs of being forced into alignment by the strong laser field even with a pulse duration of 50 fs [15]. This effect is due to the combined effects of the strong polarizability induced by the intense laser field and to the multiple ionization of the system. If one considers only the neutral molecule polarizability effects represented by the dipole moment \mathbf{p} induced by a linearly polarized laser field \mathbf{E} , the field-molecule interaction $V = -(1/2)\langle \mathbf{p} \cdot \mathbf{E} \rangle$ averaged over one optical cycle is given by the following expression as a function of time t and angle ϑ between the molecular axis and the laser field direction:

$$V(t, \vartheta) = -\frac{I(t)}{2c} [\alpha_{\parallel} \cos^2(\vartheta) + \alpha_{\perp} \sin^2(\vartheta)]. \quad (2)$$

In Eq. (2), $I(t)$, c , α_{\parallel} , and α_{\perp} are, respectively, the time-dependent laser intensity, the speed of light, and the parallel and transverse components of the polarizability tensor. These two last physical quantities depend on the laser frequency ν . However, they can be replaced, respectively, by the static parallel and perpendicular polarizabilities because the photon energy $h\nu = 1.55$ eV at $\lambda = 800$ nm remains small in comparison with the energies of the first excited states in N_2 and CO_2 that can be reached via a one-photon transition. For instance, for CO_2 at $I = 10^{15}$ W/cm 2 , $V(t, \theta)$ presents a maximum well depth of 212 meV. Assuming a classical behavior of the molecular rotation, the evolution equation of the angle $\Theta = 2\vartheta$ is given by

$$\frac{d^2\Theta}{dt^2} + \left(\frac{2\pi}{T_r}\right)^2 f(t) \sin(\Theta) = 0, \quad (3)$$

where $f(t)$ is the temporal envelope of the laser intensity $I(t) = I_{\max} f(t)$. The time constant T_r can be expressed as a function of the inertial momentum J of the molecule, the maximum laser intensity I_{\max} , and the difference $\Delta\alpha = \alpha_{\parallel} - \alpha_{\perp}$ which represents the anisotropy of the molecular polarizability:

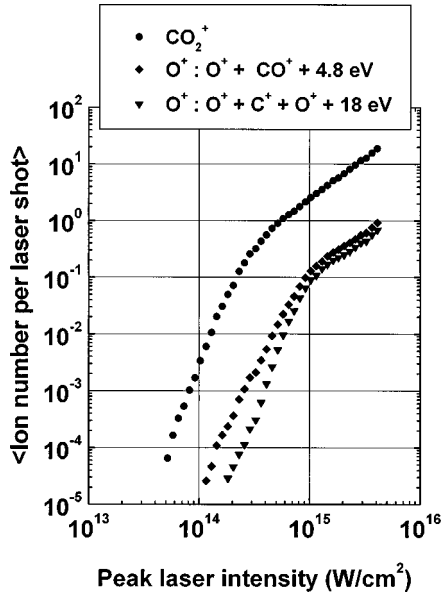


FIG. 8. Experimental CO_2^+ (●) and O^+ (◆, ▼) average ion numbers per laser shot for a reference pressure $P(\text{CO}_2) = 10^{-9}$ Torr as a function of the peak laser intensity recorded at $\lambda = 800$ nm and linearly polarized laser light. The spectrometer is equipped with grids and all the ions produced in the focal volume are detected. The O^+ ions come from two different channels: (◆) $\text{O}^+ + \text{CO}^+ + 4.8$ eV and (▼) $\text{O}^+ + \text{C}^+ + \text{O}^+ + 18$ eV.

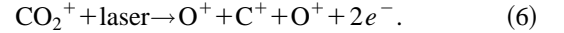
$$T_r = 2\pi \left(\frac{cJ}{I_{\max} \Delta \alpha} \right)^{1/2}. \quad (4)$$

Equation (4) gives an order of magnitude of the rotation time especially for small Θ angles where $\sin(\Theta) \approx \Theta$. At $I_{\max} = 10^{15}$ W/cm², the values of T_r are 160, 422, and 645 fs for, respectively, H₂, N₂, and CO₂. These values are much larger than the laser period $T = 2.67$ fs at $\lambda = 800$ nm and justify the average of the field-molecule interaction $V = -(1/2)\mathbf{p} \cdot \mathbf{E}$ over one optical cycle. In any case, they are much larger than the laser pulse duration 40 fs and cannot explain the molecular alignment if one takes into account only the neutral molecule polarizability. In addition, the molecular ion yields as a function of the peak laser intensity do not support the fact that only molecules aligned along the laser electric field are ionized. Figure 8 represents the CO_2^+ , O^+ from the $\text{O}^+ + \text{CO}^+ + 4.8$ eV and O^+ from the $\text{O}^+ + \text{C}^+ + \text{O}^+ + 18$ eV ion yields. For the CO_2^+ ions the saturation laser intensity is around 2×10^{14} W/cm². For intensities larger than this value, the variation of the CO_2^+ ion numbers follows the well-known $\frac{3}{2}$ slope in log-log coordinates due to the saturation of the ionization process associated with the extension of the laser focal volume. The same behavior is observed for the O^+ ions at laser intensities above 10^{15} W/cm² and is due to the saturation of the $\text{CO}_2^+ \rightarrow \text{O}^+ + \text{CO}^+ + e^-$ and $\text{CO}_2^+ \rightarrow \text{O}^+ + \text{C}^+ + \text{O}^+ + 2e^-$ ionization channels. For these two particular channels, the $\frac{3}{2}$ slope above 10^{15} W/cm² show that all the precursor CO_2^+ ions are ionized whatever their initial internuclear axis direction. The same behavior was observed with the N₂ molecule. The laser intensity dependence always shows the $\frac{3}{2}$ slope above saturation, which means that all the initial populations leading to the fragmentation channels are ionized.

Following our present analysis and the analysis of Posthumus *et al.* [15], the ionization processes have to be considered in the reorientation of light molecules in addition to the polarizability effects induced by the strong linearly polarized laser field on the neutral molecule. In Fig. 8, the O^+ ions coming from the $\text{O}^+ + \text{CO}^+ + 4.8$ eV channel exhibit a saturation knee at the same laser intensity around 10^{15} W/cm² as the O^+ ions coming from the $\text{O}^+ + \text{C}^+ + \text{O}^+ + 18$ eV channels. These two types of ions come, respectively, from the removal of two and three electrons from the molecule. The saturation of the first class of O^+ ions at 10^{15} W/cm² comes from the saturation of the ionization of the CO_2^+ ions following:



The second class of O^+ ions saturates at the same laser intensity and as a consequence the corresponding channel $\text{O}^+ + \text{C}^+ + \text{O}^+$ comes from the ionization of the same CO_2^+ precursor ions following a nonsequential two-electron emission:



The nonsequential double ionization of neutral molecules has been studied recently in our laboratory [19] and, to our knowledge, this is the first report of the nonsequential double ionization of a molecular ion. To our knowledge, the dynamics of the departing electrons has not been investigated for the molecular multiple ionization. As a consequence, its influence on the molecular rotation remains to be studied in the linear polarization case.

In circular polarization, the molecules do not have time to rotate following the laser electric field rotation during the laser period $T = 2.67$ fs at $\lambda = 800$ nm and no molecular reorientation processes are expected in this case. Using the on-axis detection described in Sec. II C, the detected fragmentation channels come only from molecules with their internuclear axis initially parallel to the detection axis. The ionization takes place in the course of the laser electric field rotation from 0° to 360° within one optical period. As a consequence, the kinetic energy releases are independent of the respective directions of the laser field and internuclear axis since they remain the same as in linear polarization. One might argue that the ionization is expected to be larger when the molecular axis is parallel to the laser field because in this case the escaping electron feels only the attracting field of one nucleus instead of the attracting field of two or more nuclei when the molecular axis is perpendicular to the laser field. The situations in linear and circular polarization are then not very different, since one particular molecular direction in space is favored. However, the ion yield measurements in circular polarization exhibit the same $\frac{3}{2}$ slope in log-log coordinates as in Fig. 8 above the laser saturation intensity. This means that all the molecules are ionized in the focal volume regardless of their initial orientation. In addition, there is no reason for the molecular axis to have exactly the same position in space in linear and circular polarization.

Another way to show the independence of the kinetic energy releases as a function of the positions of the laser field and molecular axes is illustrated in Fig. 9 for N₂. Using the on-axis detection which fixes the spatial orientation of the

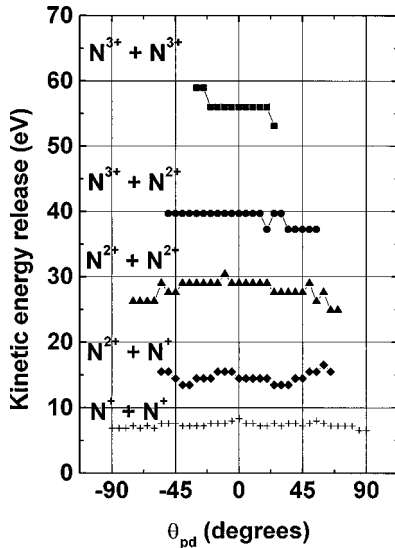


FIG. 9. Kinetic energy releases of the $N^{Z+} + N^{Z'+}$ ($Z, Z' = 1, 2, 3$) fragmentation channels of N_2 recorded at $\lambda = 800$ nm, $I = 3.5 \times 10^{15}$ W/cm 2 , and $p(N_2) = 10^{-8}$ Torr, as a function of the angle ϑ_{pd} between the linear laser polarization direction and the spectrometer axis, i.e., the molecular explosion direction. The spectrometer is equipped with a 1 mm pinhole for an on-axis detection and the collection electric field is $F_c = 100$ V/cm.

exploding molecules, the linearly polarized laser field direction is rotated from $\vartheta_{pd} = -90^\circ$ to $\vartheta_{pd} = 90^\circ$, where ϑ_{pd} is the angle between the laser field direction and the spectrometer axis, i.e., the molecular explosion direction. Then the kinetic energy releases are recorded for each angle ϑ_{pd} while the laser intensity $I = 3.5 \times 10^{15}$ W/cm 2 remains constant. In Fig. 9, no significant variation is noticeable for all the $N^{Z+} + N^{Z'+}$ ($Z, Z' = 1, 2, 3$) channels. The only slight variation occurs at angles $|\vartheta_{pd}| > 45^\circ$ for $N^{2+} + N^{2+}$ and $|\vartheta_{pd}| > 25^\circ$ for $N^{3+} + N^{3+}$. This is due to the fact that the corresponding angular distributions are peaked at $\vartheta_{pd} = 0^\circ$ with a half-width at half maximum of 15° and 12° for, respectively, the $N^{2+} + N^{2+}$ and $N^{3+} + N^{3+}$ channels with the 1 mm pinhole. The signals at $|\vartheta_{pd}| > 45^\circ$ for $N^{2+} + N^{2+}$ and $|\vartheta_{pd}| > 25^\circ$ for $N^{3+} + N^{3+}$ are much weaker than at $\vartheta_{pd} = 0^\circ$ and as a consequence the accuracy of the measurements are lower than at $\vartheta_{pd} = 0^\circ$. Similar results were obtained with the CO_2 molecule for the channels reported in Table II. As a consequence, our overall results show that the molecular relaxation is independent of the relative positions of the laser electric field and the internuclear axis.

Double pulse experiments have proven the molecular reorientation of the equivalent CO molecule using a 1 ps laser pulse [13]. With very short pulses of 50 fs duration, Posthumus *et al.* have shown that the reorientation is effective for light molecules such as H_2 or N_2 [15]. The first group of models presented in the Introduction predicts an enhancement of the multiple ionization at large internuclear distances in linear polarization [7–10]. The stretching processes leading to these distances remain unknown and one of the possible mechanisms could be inertial forces due to the forced rotation of the molecules. However, our results show that this is not the case for two reasons. Inertial forces are absent in the circular polarization case, which gives the same kinetic energy releases as in the linear case. Moreover, as it is shown above, the kinetic energy releases do not depend on the angle between the laser electric field and the internuclear direction.

V. CONCLUSIONS

In the Introduction of this paper, several theoretical approaches were presented in order to give the motivations of this experimental work. In particular, the theories predicting an enhancement of the multiple ionization at large internuclear distances [7–10] are not compatible with the Thomas-Fermi approach [11,12] within our present understanding of multiple ionization of molecules. The experimental results presented in this paper and in particular those obtained with circularly polarized laser light should constitute additional tests of the models since no data were available in this case. This could be done increasing the computation time since the directions of the laser field and internuclear axes have to be independent in order to predict the dynamics of the ionization as a function of these directions and to be able to get more insight into the nuclear motions in linear and circular polarization. In addition, the electron departure dynamics is known to be very sensitive to the laser polarization states. Our results show that the fragmentation dynamics does not seem to be correlated to the electronic emission in strong laser fields since the fragmentation kinetic energy releases do not depend on the laser polarization.

ACKNOWLEDGMENTS

The authors are pleased to acknowledge M. Bougeard and E. Caprin (CEA/DSM/DRECAM/SPAM) for their skilled technical assistance, and G. Vigneron (CEA/DSM/DRECAM/SCM) for his expertise of the kHz titanium sapphire laser system.

-
- [1] L. J. Frasinski, K. Codling, P. Hatherly, J. Barr, I. N. Ross, and W. T. Toner, *Phys. Rev. Lett.* **58**, 2424 (1987).
 - [2] C. Cornaggia, J. Lavancier, D. Normand, J. Morellec, P. Agostini, J.-P. Chambaret, and A. Antonetti, *Phys. Rev. A* **44**, 4499 (1991).
 - [3] K. Codling, C. Cornaggia, L. J. Frasinski, P. A. Hatherly, J. Morellec, and D. Normand, *J. Phys. B* **24**, L593 (1991).
 - [4] C. Cornaggia, D. Normand, and J. Morellec, *J. Phys. B* **25**, L415 (1992).
 - [5] M. Schmidt, D. Normand, and C. Cornaggia, *Phys. Rev. A* **50**, 5037 (1994).
 - [6] P. A. Hatherly, M. Stankiewicz, K. Codling, L. J. Frasinski, and G. M. Cross, *J. Phys. B* **27**, 2993 (1994).
 - [7] J. H. Posthumus, L. J. Frasinski, A. J. Giles, and K. Codling, *J. Phys. B* **28**, L349 (1995).
 - [8] T. Seideman, M. Yu. Ivanov, and P. B. Corkum, *Phys. Rev. Lett.* **75**, 2819 (1996).
 - [9] T. Zuo, S. Chelkowski, and A. Bandrauk, *Phys. Rev. A* **48**, 3837 (1993).
 - [10] S. Chelkowski and A. Bandrauk, *J. Phys. B* **28**, L723 (1995).
 - [11] M. Brewczyk, C. W. Clark, M. Lewenstein, and K. Rzazewski,

- Phys. Rev. Lett. **80**, 1857 (1998).
- [12] M. Brewczyk, C. W. Clark, and K. Rzazewski (unpublished).
- [13] D. Normand, L. A. Lompré, and C. Cornaggia, J. Phys. B **25**, L497 (1992).
- [14] D. Normand and C. Cornaggia, *Super-Intense Laser-Atom Physics*, edited by B. Piraux, A. L'Huillier, and K. Rzazewski (Plenum, New York, 1993), p. 351.
- [15] J. H. Posthumus, J. Plumridge, M. K. Thomas, K. Codling, L. J. Frasinski, A. J. Langley, and P. F. Taday, J. Phys. B **31**, L553 (1998).
- [16] W. C. Wiley and I. H. McLaren, Rev. Sci. Instrum. **26**, 1150 (1955).
- [17] L. J. Frasinski, K. Codling, and P. A. Hatherly, Phys. Lett. A **142**, 499 (1989).
- [18] C. Cornaggia, Phys. Rev. A **54**, R2555 (1996).
- [19] C. Cornaggia and Ph. Hering, J. Phys. B **31**, L503 (1998).